## Application of LWIR Spectro-Polarimetry for Ice-Water Discrimination

Discriminating between the thermodynamic phases of water is relevant for many environmental science applications. Earth's cryosphere is changing rapidly, and melting sea ice can affect large-scale ocean circulation patterns that change the global environment. The detection of melt ponds, pools of open water that form on sea ice surfaces, is an area where typical LWIR imaging falls short due to the water being at a similar temperature to the surrounding ice. However, solid ice and liquid water at the same physical temperature will exhibit different polarimetric properties. Therefore, LWIR polarimetric imaging is potentially useful for ice-water discrimination. Investigating this assertion requires knowledge of: 1) optical physics to explain differences in polarized LWIR spectra of ice and water, 2) optical engineering to design a polarimeter capable of observing these differences, and 3) image science to retrieve estimates of spectro-polarimetric information from measurements.

# 1 Optical Physics: Background

## 1.1 Polarization in LWIR

The polarization of light describes the oscillation of the transverse electric field. Broadband light can be fully polarized, partially polarized, or unpolarized [1]. The linear Stokes parameters uniquely quantify the polarization of light with four real-valued numbers: $I, Q, U$, here $I$ describes the total intensity of light. Unpolarized light reflected or transmitted through a material can become polarized as a result of Fresnel interactions at the optical interfaces. Light polarized perpendicular to the plane of incidence is called s-polarization, whereas light polarized parallel to the plane of incidence is called p-polarization. The Fresnel intensity coefficients represent the magnitude of the reflected and transmitted field relative to the magnitude of incident light. The reflection intensity coefficients for s and p-polarization depend on the incident and refractive indices, the incident angle, and the refracted angle [1, 2].

Evaluation of the Fresnel equations will show that the reflection coefficient for the s-polarization is larger than the p-polarization coefficient at most view angles. Therefore, when unpolarized light is incident, the reflected light is more s-polarized, and the transmitted light is more p-polarized. In the long-wave infrared (LWIR) waveband, light becomes polarized from both reflection and emission. Emission can be thought of as transmission to the surface from inside the material; therefore,

emission is also mostly p-polarized. A blackbody is an idealization of a material that absorbs all radiation incident upon it. When a blackbody is at thermal equilibrium at temperature T, the material will emit spectral radiance described by Planck's law,

$$B(\nu, T) = \frac{2h\nu^3}{c^2 \exp(\frac{h\nu}{k_b T}) - 1} \tag{1}$$

here $\nu$ is the frequency of the emitted radiation, $k_B$ is the Boltzmann constant, $c$ is the speed of light, and $h$ is Planck's constant. Emissivity is the effectiveness of an object emitting energy as thermal radiation; therefore, blackbodies have an emissivity of 1 whereas perfect reflectors have an emissivity of 0. For a blackbody at thermal equilibrium, emission is unpolarized because all the incoming radiation that is absorbed is completely re-emitted without a preferential direction. "Graybodies" have an emissivity $< 1$, so the emission will be partially polarized at view angles other than normal incidence because there will be some radiation reflected back into the medium as opposed to being completely transmitted to the surface.

Kirchoff's law of thermal radiation expresses that the emissivity of a freely radiating body is equal to its absorption. To conserve energy in light-matter interactions, reflectivity, transmittance, and absorption sum to unity [3]. For an opaque medium, the transmission is negligible. Therefore, water, which is opaque in the LWIR, has a polarized emissivity that can be described as $e_{s,p} = 1 - R_{s,p}$, where $R_{s,p}$ are the Fresnel reflection coefficients, so the emissivity is dependent on the refractive index and the view angle [4]. Finally, the polarization difference (PD), a quantity that describes the magnitude of polarization, is defined as PD=$\frac{e_s - e_p}{e_s + e_p}$ for emission polarization [4]. It can also be described as PD=$\frac{R_s - R_p}{R_s + R_p}$ for reflection polarization.

Thermal polarimetry depends on:the material's emissivity, view geometry, and its kinetic temperature relative to the scene background. The spectral radiance of the object shown in Fig. 1 can be modeled as $L_{object}(\nu, \theta) = B(\nu, T_o)\varepsilon(\theta) + B(\nu, T_b)r(\theta)$. Here, $B(\nu, T)$ is Planck blackbody radiation at temperature $T$ from Eq. 1, $\varepsilon$ and $r$ are the emissivity and reflectivity, respectively. For a graybody, $L_{object}(\nu, T)$ would always be less than $B(\nu, T)$ for the same frequency and kinetic temperature. The temperature at which an ideal blackbody would need to be in order to have an equivalent radiance of a graybody at a given wavelength is called the brightness temperature.

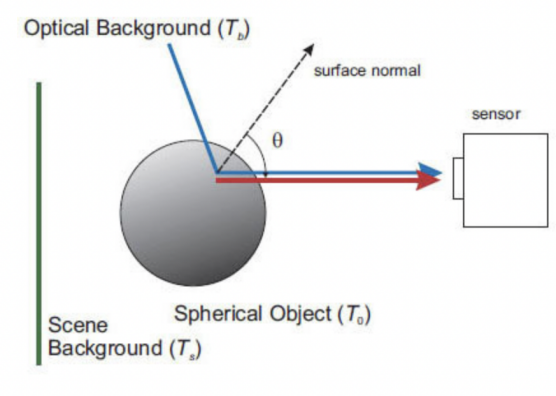


Figure 1: Geometry for LWIR emission and reflection from a spherical object [5]. The arrows show the direction of the reflection of the optical background ($T_b$ in blue) and emission of object radiance ($T_o$ in red).

For greybodies, the brightness temperature is always less than its kinetic temperature, and the ratio between the two is another way to describe emissivity [6]. In LWIR imaging, brightness temperature is used as a measure of radiance and is reported in units of Kelvin.

When the object is significantly colder than its optical background ($T_b >> T_o$), the polarization signature is dominated by reflections of the background radiation off the object surface, *i.e* the $B(\nu, T_b)r(\theta)$ term dominates the spectral radiance in the $L_{object}$ equation given above. When the object is much hotter than the optical background ($T_o >> T_b$), the polarization signature is dominated by the emitted radiation from the surface. Most LWIR polarimetric sensors are designed for this operating case. However, when the object is in thermal equilibrium, *i.e* the object's temperature is equal to the optical background, reflection and emission equally contribute to the total radiance leaving the object. Therefore, it is possible to eliminate the polarization signature because the orthogonal emission and reflection polarization states combine to create unpolarized light on the sensor [5].

## 1.2 Optical Constants of Water

Many liquids, such as water, are composed of molecules that have permanent electric dipole moments. In the absence of an external field, the ensemble dipole orientation is randomly distributed. However, in the presence of an external field, water absorbs radiation to reorient the molecules. The dipoles attempt to align to the external field, and an opposing restoring force is created. The process in which the dipoles "relax" to equilibrium while under the influence of this restoring force is called Debye relaxation [2]. This relaxation time is highly temperature-dependent. In the phase transition from liquid to solid water, the electric dipoles in the liquid lose their orientational mobility and are unable to reorient themselves in the solid. Therefore, as the water kinetic temperature decreases,

the Debye relaxation vanishes. Dipole relaxation is the source of the high absorption of water in the microwave and infrared regions [2].

Molecular vibrations are another dominant mechanism for absorption in the LWIR. Fundamental vibration modes of the $H_2O$ molecule occur at different frequencies, which correspond to the peak absorption wavelengths of ice and water. Ice and water have different vibrational frequencies because as water freezes and molecules are locked into a lattice structure, the vibrations slow down. Therefore, ice will have lower resonant vibrational frequencies and absorption peaks at longer wavelengths.

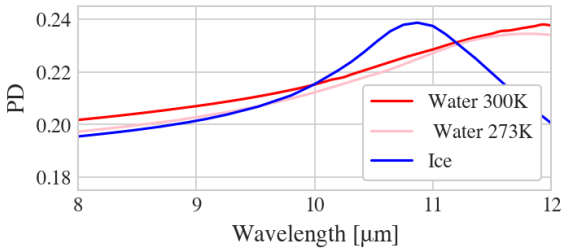


Figure 2: Polarization difference at 20° view angle. Calculated from Fresnel reflectivity coefficients. Wavelength-dependent refractive index information obtained from a public database [7].

These physical processes result in different refractive indices for liquid and solid water. The Fresnel coefficients depend on the viewing geometry and refractive index. The polarization difference, calculated with Fresnel reflection coefficients, is plotted as a function of wavelength in Fig. 2 from 8-12$\mu$m. There are notable differences in the magnitude of polarization of ice and water at $273K$. At the freezing point of water ($273K$), a phase transition occurs between liquid and solid water. Although solid ice and liquid water at $273K$ may be nearly identical in kinetic temperature, the spectral polarization signatures are different [8].

Because the contrasting polarizations of ice and water are due to spectral differences in the refractive indices, there is a need for an instrument to measure the polarization magnitude as a function of wavelength: a linear channeled spectro-polarimeter (LCSP). Fig. 2 provides insight into the polarimetric precision and spectral resolution needed to resolve these differences. The PD values of ice and water at $273K$ are approximately equal at 9.5 $\mu$m. The largest difference in PD between these two samples is approximately 0.015 at 10.7 $\mu$m. Therefore, there is a need for a LWIR spectro-polarimeter that has a polarimetric precision capable of resolving a 1.5% difference in polarization and has a spectral resolution of at least 1.2$\mu$m in order to resolve a difference between 9.5 and 10.7 $\mu$m.

# 2 Optical Engineering: Spectro-Polarimeter Design

The Polarization Lab developed an Infrared Channeled Spectro-Polarimeter (IRCSP). The IRCSP instrument concept was based on the SPEX airborne spectro-polarimeter design [9, 10]. All channeled polarimeters must implement three major steps: introduce a wavelength dependence on the input angle of linear polarization (AoLP), modulate the rotated AoLP, and spectrally resolve the intensity [9, 11]. For the first step, channeled polarimeters typically take advantage of the wavelength dependence of high-order retarders. The incoming polarized light will rotate by an amount dictated by the retardance. The phase of the modulation will then depend on the AoLP and the carrier frequency introduced by the retarder. To implement the second step, a polarizing beam-splitter element is used to create two channels. The relative signal between these two channels and the amplitude of the modulation will depend on the degree of linear polarization (DoLP) of the incoming state. Unpolarized light will be evenly split between the two paths. Finally, the last step is to spectrally resolve the intensity, which is done in both the IRCSP and SPEX polarimeter with a diffraction grating. The Stokes parameters have now been encoded into intensity modulations at the focal plane. The major design considerations for an LCSP include selecting the proper retarder thickness and diffraction grating for the desired modulation frequency and selecting the polarizing beam splitter element, which affects the overall transmission of the system.

## 2.1 High-Order Retarder Thickness and Diffraction Grating

The retardance and the groove density of the diffraction grating must be selected so that the modulation period at the focal plane (in units of length) is at least twice the sampling interval. In frequency terms, the modulation frequency (in units of inverse length) must be less than half the focal-plane sampling frequency. This minimum sampling frequency is called the Nyquist rate. If the modulation frequency is above this threshold, the signal will be aliased, meaning that the true frequency of modulation cannot be uniquely reconstructed.

The modulation frequency at the focal plane will depend on the retardance of the high-order retarder (HOR) and the dispersion of the diffraction grating. Retardance can be represented in several different units. A high-order retarder (HOR) with birefringence $\Delta n(\lambda)$ and thickness $t_{HOR}$

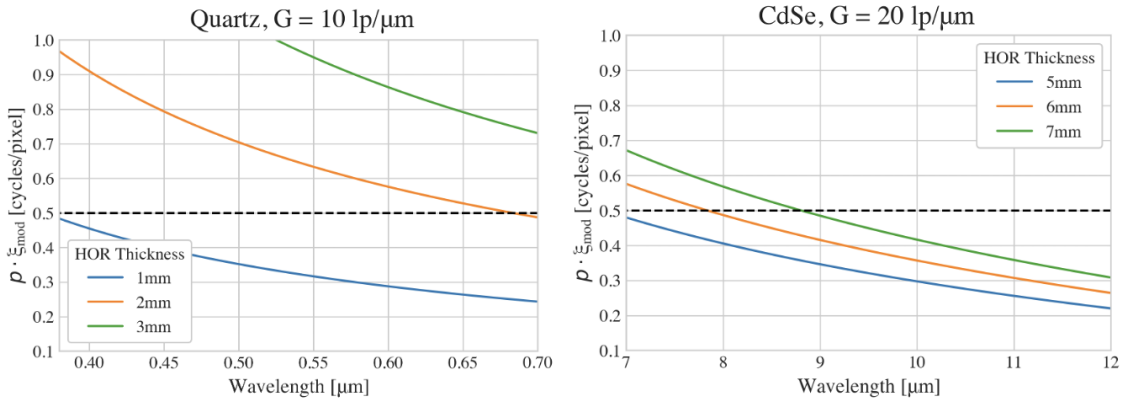


Figure 3: Modulation frequency created by two different retarders at the focal plane of a 12$\mu$m pixel pitch and 6.3mm focal plane camera. Two different retarder materials require different thicknesses and groove densities $G$ in order to be below the Nyquist rate. On the left, a quartz retarder in the visible waveband is plotted. On the right, a CdSe retarder in the LWIR waveband is plotted. Pixel pitch ($p$) multiplied by $\xi_{mod}$ must be less than 0.5 or else the frequencies will be aliased. $\xi_{mod}$ is equal to left-hand side of Eq. 2.

has retardance that can be expressed as: $\delta = \Delta n(\lambda) \cdot t_{HOR}$ in units of optical path length or $\delta = \frac{\Delta n(\lambda) \cdot t_{HOR}}{\lambda}$ in units of waves.

A diffraction grating integrated in a spectrometer with effective focal length $f$ will have a change in wavelength corresponding to a change in the lateral distance on the focal plane given by $\frac{\cos(\theta_d)}{Gf}$, where $\theta_d$ is the diffracted angle, $G$ is the grating groove density in units of lp/$\mu$m. The linear dispersion of the grating multiplied by the retardance in units of waves will give the frequency of the modulation at the focal plane. The number of samples per unit length is limited by the pixel pitch ($p$) of the detector. Pixel pitch is the distance between the center of one pixel and the center of another. The material and thickness of the retarder and the grating groove density must be selected such that

$$\frac{\Delta n(\lambda) \cdot t_{HOR}}{\lambda} \cdot \frac{\cos(\theta_d)}{Gf} [lp/\mu m] \leq 0.5 \cdot p^{-1} [1/\mu m] \tag{2}$$

Fig. 3 is a demonstration of this engineering consideration. The SPEX polarimeter uses a quartz retarder, which is a commonly used retarder material for the visible waveband. The IRCSP uses a CdSe retarder, which has birefringence in the LWIR waveband. To implement either a quartz or CdSe retarder into a spectro-polarimeter, different HOR thicknesses and diffraction gratings with different groove densities were required to get the modulation frequency below half the focal plane

sampling frequency. This demonstration for both retarders was done considering a system with a pixel pitch of 12$\mu$m and focal length 6.3mm, but these detector parameters could also be adjusted to tune the frequency. For example, to further decrease the modulation frequency, the focal length of the imaging system should be increased.

## 2.2 Alignment with Quarter Wave Retarder

Another design consideration is the addition of a second retarder. A single high-order retarder is not enough to modulate the linear Stokes parameters [10]. Before the HOR must be a quarter wave plate (QWP) with its fast axis 45° relative to the HOR's fast axis. Without this QWP, there would be two polarization states, the eigenpolarizations of the HOR corresponding to the fast and slow axes, which would pass through the HOR unchanged and would not be modulated with respect to wavelength. For example, if there was no QWP and the HOR had a fast axis of 135°, then the second Stokes parameter $U$, which describes the 45° and 135° states, could not be measured because incoming polarized radiance with an AoLP of 135° would not be modulated. With the QWP, the two retarders become one with elliptical eigenstates. If the spectro-polarimeter is designed to measure only linear states, this is acceptable.

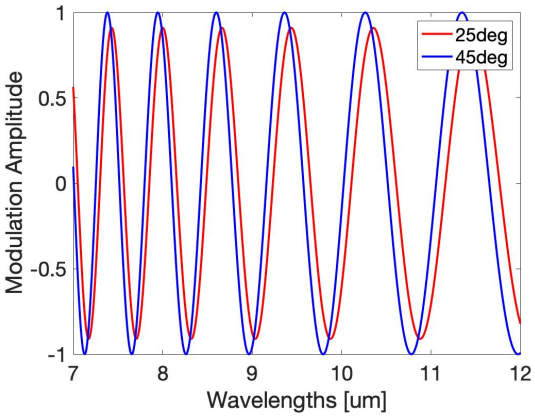


Figure 4: Simulated noise-free modulation function (see Eq. 4) at 90° AoLP. The fast-axes of the high-order retarder and quarter-wave plate are 25° (red) or 45° (blue) apart. This alignment affects polarimetric efficiency (see Eq. 4).

System performance can be significantly affected if this QWP is not properly aligned with the HOR. Fig. 4 shows a noise-free simulated modulation function of the IRCSP. The modulation function is the difference over the sum of intensity in the two paths. For a perfect system, the modulation amplitude will be bound between [-1,1], as is for the curve representing the HOR and QWP fast axes 45° apart in Fig. 4. The polarimetric efficiency decreases when that relative angle changes, as shown in the decrease in modulation amplitude at 25° relative fast axis in Fig. 4. A slight decrease

in system performance is expected with a misalignment and will be further exaggerated with the noise introduced.

## 2.3 Polarized Beam Splitter

The biggest factors when selecting this component are the transmission spectrum and the contrast ratio between orthogonal polarization states. The SPEX airborne spectro-polarimeter uses a Wollaston prism, which enables imaging of both paths on the same detector with a chosen angular separation [10]. A major design consideration for the use of Wollaston prisms is the wavelength dependence on the splitting angle [10, 11]. As an example, for a Calcite Wollaston prism with a nominal split angle of 20°, the ordinary ray split angle would be 10.13° at 400 nm. For an extraordinary ray, the split angles would be $-11.45°$ for 400 nm and $-10.04°$ for 1000 nm [11]. Therefore, for a spectro-polarimeter designed to operate between 400-1000nm, the two diffraction gratings following the beam splitter should be able to accept a range of angles beyond just the nominal split angle of $\pm 10°$ in order to prevent vignetting of the shortest and longest wavelengths. Furthermore, the Wollaston prism will have different nominal splitting angles for s- and p-polarized beams. In the SPEX polarimeter, there is a smaller field of view for the s-beam and therefore more light per pixel captured in that channel. Because the relative signal between the orthogonal channels is how DoLP is determined, this difference should be taken into account during calibration.

In the IRCSP, a wire grid polarizer acts as the polarized beam splitter element [12, 13]. Due to size constraints, a Wollaston prism in the required spectral range of 8-12$\mu$m was not feasible, although it was the preferred choice due to its high transmission across the waveband. Wire grid polarizers work by reflecting the field parallel to the wire. The blocked polarization state will be completely reflected, but the state perpendicular to the wires will not be perfectly transmitted. The contrast ratio between the reflected and transmitted state is also wavelength-dependent. Due to this effect, the IRCSP has a similar problem as the SPEX. The IRCSP channel that receives the reflected state has a higher signal than the path with the transmitted state. Additionally, the transmission through the polarizer will depend on the AoLP. The variation in contrast for both unpolarized and polarized input needs to be characterized in calibration in order to implement a correction factor.

# 3 Image Science: Data Reduction

The analytic expression for the continuous modulation function is calculated using the Mueller matrix model of the polarimeter. A Mueller matrix represents linear light-matter interactions between an incoming and outgoing Stokes vector. The system Mueller matrix in the s- and p-polarized paths is the concatenated Mueller matrix of the polarized beam splitter ($M_{PBS,\ s/p}$), the high order retarder ($M_{HOR}$), and the quarter wave plate ($M_{QWP}$). The IRCSP intensity on the detector in each of the two paths is described by

$$I_{s/p}(\lambda) = \frac{I(\lambda)}{2}\left[1 \pm D\sin\left(\frac{2\pi\delta(\lambda)}{\lambda}\right) + 2\theta)\right] \tag{3}$$

where $\delta(\lambda)$ is the retardance, D is the DoLP and $\theta$ is the AoLP. As stated above, the modulation function is then calculated as the normalized difference in intensity of the two paths $(I_s - I_p)/(I_s + I_p)$ which simplifies to

$$M_\lambda = W_{\theta,\lambda}\left[Q\sin\left(\frac{2\pi\delta(\lambda)}{\lambda}\right) + U\cos\left(\frac{2\pi\delta(\lambda)}{\lambda}\right)\right]. \tag{4}$$

Here $Q$ and U are Stokes parameters and $W_{\theta,\lambda}$ is a unitless parameter in the range of [-1,1] denoted the polarimetric efficiency. $W_{\theta,\lambda}$ describes that reduction in modulation and quantifies how sensitive the instrument is to changes in polarization. The point spread function associated with the lens and stop of the imaging system will blur the modulation function due to diffraction and optical aberrations.

With broadband input light, the signal is spectrally blurred. At lower wavelengths, this effect is even greater because the period of modulation is smaller. Therefore, there are fewer pixels and a higher spatial frequency on the focal plane, so the signal at lower wavelengths is more susceptible to noise. This is the source of the wavelength dependence on the efficiency term, because polarimetric efficiency decreases with wavelength. The AoLP dependence on $W_{\theta,\lambda}$ is due to the polarization-dependent transmission through the wire-grid polarizer.

The process of extracting Stokes parameters $I$, $Q$, and $U$ from discrete camera counts is called demodulation. The SPEX polarimeter uses a linear regression algorithm to retrieve $Q$ and $U$ as the fit parameters of the modulation function [10]. The IRCSP, on the other hand, does demodulation

in Fourier space to reduce the effect of noise in the system.

A Fourier transform is a method that converts a signal to its frequency domain. It decomposes a signal into its constituent sinusoidal components, identifying the different frequencies and their associated amplitudes and phases. Therefore, Fourier analysis is particularly useful for periodic functions because a sum of sinusoids will have a Fourier transform consisting of a sum of delta functions at the frequencies of the sinusoids. For the IRCSP, demodulation is done for one period of modulation, centered around a given wavelength. One full period is needed to reconstruct the amplitude and phase information needed for the DoLP and AoLP retrieval.

A power spectrum identifies the frequency content of a signal. The power spectrum is the modulus squared of the discrete Fourier transform, and it results in a real-valued function that quantifies the contribution of each frequency to the total signal. A signal with high noise content will have larger frequency terms, and thus will have a wider power spectrum.

The most prevalent source of noise in the uncooled microbolometers used in the IRCSP is Johnson noise, which describes the random motion of charge carriers and results in a detector response that changes with focal plane temperature fluctuations. The uncooled microbolometers have a reported Noise Equivalent Differential Temperature (NEDT) of $< 40mK$. This is the change in scene temperature that will result in a change in detector response greater than the signal-to-noise ratio. In other words, the minimum resolvable change in scene temperature. The NEDT of the IRCSP is wavelength-dependent and typically higher than the NEDT of the detectors alone because of the reduced transmission introduced by the polarization elements. The NEDT can be improved by cooling the instrument.

Johnson noise has a higher spatial frequency compared to the frequency of one period of modulation, so the power spectrum of Johnson noise will be much wider than the IRCSP power spectrum. Using a power spectrum to identify the present frequency of one period of modulation effectively filters out the larger frequency terms that are present because of Johnson noise contribution. This effect is why IRCSP demodulation is done in the Fourier domain.

Finally, DoLP and AoLP are calculated from the Stokes parameters using the following relations: $DoLP = \sqrt{Q^2 + U^2}/I, AoLP = tan^{-1}(U/Q)$.

# References


[1] Russell A Chipman, Wai Sze Tiffany Lam, and Garam Young. *Polarized light and optical systems*. CRC Press, 2018.

[2] Craig F Bohren and Donald R Huffman. *Absorption and scattering of light by small particles*. John Wiley & Sons, 2008.

[3] Nathan Hagen. "Review of thermal infrared polarimetry, I: theory". In: *Optical Engineering* 61.7 (2022), p. 070902.

[4] Joeseph A. Shaw and Christopher Marston. "Polarized infrared emissivity for a rough water surface". In: *Appl. Opt.* 7 (2000), pp. 375–380. DOI: 10.1364/OE.7.000375.

[5] J Scott Tyo, Bradley M Ratliff, James K Boger, Wiley T Black, David L Bowers, and Matthew P Fetrow. *The effects of thermal equilibrium and contrast in LWIR polarimetric images*. https://opg.optica.org/oe/fulltext.cfm?uri=oe-15-23-15161&id=144634. (2007).

[6] Andrew Resnick, Chris Persons, and George Lindquist. "Polarized emissivity and Kirchhoff's law". In: *Applied optics* 38.8 (1999), pp. 1384–1387.

[7] Mikhail N. Polyanskiy. *Refractive index database*. https://refractiveindex.info. 2008.

[8] Jaclyn A. John, Jeremy C. Parkinson, and Meredith K. Kupinski. "Differences in ice and water LWIR spectral polarimetry at room temperature". In: *Polarization Science and Remote Sensing XI* 12690 (2023). URL: https://doi.org/10.1117/12.2678064.

[9] Kira A. Hart, Russel A. Chipman, and Dong L. Wu. "Compact LWIR polarimeter for cirrus ice properties". In: *Polarization: Measurement, Analysis, and Remote Sensing XIII* 10655 (2018), p. 106550V.

[10] J Martijn Smit, Jeroen HH Rietjens, Gerard van Harten, Antonio Di Noia, Wouter Laauwen, Brian E Rheingans, David J Diner, Brian Cairns, Andrzej Wasilewski, Kirk D Knobelspiesse, et al. "SPEX airborne spectropolarimeter calibration and performance". In: *Applied optics* 58.21 (2019), pp. 5695–5719.

[11] Nathan Hagen. "Design of channeled spectropolarimeters". In: *Applied Optics* 61.12 (2022).

[12] Kira A. Hart, Dong L. Wu, Russell A. Chipman, and Meredith K. Kupinski. "Stokes resolved differential temperature: an important metric of polarimetric precision in the long-wave infrared". In: (2021).

[13] Kira A. Shanks, Jaclyn A. John, Jeremy C. Parkinson, Dong L. Wu, and Meredith K. Kupinski. "High-altitude demonstration of LWIR polarimeter using uncooled microbolometer". In: *Journal of Quantitative Spectroscopy and Radiative Transfer (JQSRT)* (in review) (2023).